Nanoscale

PAPER

View Article Online
View Journal | View Issue

Cite this: *Nanoscale*, 2018, **10**, 1788

Using PEGylated magnetic nanoparticles to describe the EPR effect in tumor for predicting therapeutic efficacy of micelle drugs†

Ling Chen,‡[a] Fengchao Zang,‡[b] Haoan Wu,[a] Jianzhong Li,[c] Jun Xie,[a,d] Ming Ma,[a] Ning Gu *[a] and Yu Zhang *[a]

Micelle drugs based on a polymeric platform offer great advantages over liposomal drugs for tumor treatment. Although nearly all of the nanomedicines approved in the clinical use can passively target to the tumor tissues on the basis of an enhanced permeability and retention (EPR) effect, the nanodrugs have shown heterogenous responses in the patients. This phenomenon may be traced back to the EPR effect of tumor, which is extremely variable in the individuals from extensive studies. Nevertheless, there is a lack of experimental data describing the EPR effect and predicting its impact on therapeutic efficacy of nanoagents. Herein, we developed 32 nm magnetic iron oxide nanoparticles (MION) as a T_2-weighted contrast agent to describe the EPR effect of each tumor by *in vivo* magnetic resonance imaging (MRI). The MION were synthesized by a thermal decomposition method and modified with DSPE-PEG2000 for biological applications. The PEGylated MION (Fe_3O_4@PEG) exhibited high r_2 of 571 mM^{-1} s^{-1} and saturation magnetization (M_s) of 94 emu g^{-1} Fe as well as long stability and favorable biocompatibility through the *in vitro* studies. The enhancement intensities of the tumor tissue from the MR images were quantitatively measured as TNR (Tumor/Normal tissue signal Ratio) values, which were correlated with the delay of tumor growth after intravenous administration of the PLA-PEG/PTX micelle drug. The results demonstrated that the group with the smallest TNR values (TNR < 0.5) displayed the best tumor inhibitory effect. In addition, there was a superior correlation between TNR value and relative tumor delay in individual mice. These analysis results indicated that the TNR value of the tumor region enhanced by Fe_3O_4@PEG (d = 32 nm) could be used to predict the therapeutic efficacy of the micelle drugs ($d \leq 32$ nm) in a certain period of time. Fe_3O_4@PEG has a potential to serve as an ideal MRI contrast agent to visualize the EPR effect in patients for accurate medication guidance of micelle drugs in the future treatment of tumors.

Received 8th November 2017,
Accepted 17th December 2017

DOI: 10.1039/c7nr08319j

rsc.li/nanoscale

Introduction

The new interdisciplinary field termed "nanomedicine" emerged as early as the 1990s and was defined as the use of nanoscale- or nanostructured-materials in medicine due to their structure having unique medical effects.[1] In the recent years, considerable efforts were made in the drug delivery system through nanocarriers, particularly in cancer therapy. Several nanotherapeutics have been approved for the treatment of various solid tumors in the clinic; these include albumin–paclitaxel nanoparticles (Abraxane®), liposomal daunorubicin (DaunoXome®), and PEGylated liposomal doxorubicin (Doxil® and Caelyx®), while few others are in preclinical or clinical trials.[2,3] Since these anti-tumor nano-drugs are not likely to be able to penetrate deeply into the tumor interstitial matrix due to their relatively large sizes (100–200 nm),[4] the drug-loading polymeric micelles with smaller size and superior anti-tumor efficacy have been reported by researchers.[5–7] The polymeric platform, PLA-PEG taxol, with the trade name Genexol-PM has been approved in Korea for the treatment of metastatic breast cancer and non-small cell lung cancer.[8,9] Therefore, the micelle drugs are believed to be promising in cancer chemotherapy.

[a]*State Key Laboratory of Bioelectronics, Jiangsu Key Laboratory for Biomaterials and Devices, School of Biological Science and Medical Engineering & Collaborative Innovation Center of Suzhou Nano Science and Technology, Southeast University, Nanjing 210096, P. R. China. E-mail: zhangyu@seu.edu.cn*
[b]*Jiangsu Key Laboratory of Molecular and Functional Imaging, Medical School, Southeast University, Nanjing 210096, P. R. China*
[c]*Department of Nephrology, The First Affiliated Hospital of Soochow University, Suzhou 215006, P. R. China*
[d]*School of Life Science, Jiangsu Normal University, Xuzhou 221116, P. R. China*
†Electronic supplementary information (ESI) available. See DOI: 10.1039/c7nr08319j
‡These authors contributed equally to this work.

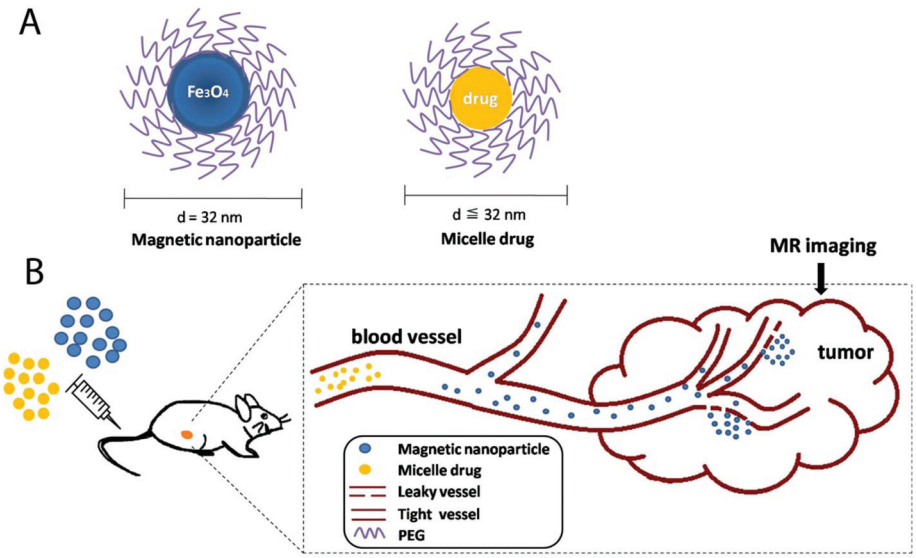

Scheme 1 (A) Structure of a magnetic nanoparticle and a micelle drug. (B) Schematic diagram showing the description of the EPR effect in tumor by MR imaging using magnetic nanoparticles for predicting the therapeutic efficacy of micelle drugs with the smaller sizes.

Nanomedicine can passively accumulate in the tumor tissue owing to the enhanced permeability and retention (EPR) effect, which is the basis for a nano-drug delivery system.[10] Nevertheless, tumor EPR effect substantially varies on different individuals and even on the same individual at different time-periods,[11,12] thus resulting in diverse tumoral accumulation of nanomedicine.[13] It can be inferred that the EPR effect may have an impact on the clinical efficacy of the anti-tumor nano agents. Thus, effectively matching the cancer patients with the novel micelle drugs according to the EPR effect is still a challenge.

Among the different types of nanomaterials, magnetic iron oxide nanoparticles (MION), which serve as the T_2-weighted magnetic resonance imaging (MRI) contrast agents, have been widely employed for the medical applications, particularly for tumor imaging.[14–17] However, all of the FDA-approved MION-based contrast agents are produced by a classic hydrolytic synthetic route, which results in poor morphology, broad size distribution, and relatively low crystallinity.[18] With the introduction of the thermal decomposition method, the resultant iron oxide nanoparticles presented monodispersity as well as higher crystallinity in addition to favorable morphology and controlled size,[19–21] thus offering great advantages for producing high-performance contrast agents. Since the bare MION are hydrophobic, further surface modification with the FDA-approved biocompatible materials such as DSPE-PEG is needed to make the MION water-soluble for the biological applications. Furthermore, PEGylation allows the MION to have surface characteristics similar to a long-circulation nanomedicine, Genexol-PM, composed of PLA-PEG. Although ferumoxytol (20 nm), which has been approved for the treatment of iron deficiency, served as the companion magnetic nanoparticles (MNP) for predicting the efficacy of the therapeutic nanoparticles (TNP, 100 nm),[22] different surface materials and large size discrepancy between MNP and TNP may have some adverse influences.

The goal of this study was to develop PEGylated MION (Fe_3O_4@PEG) and determine whether the MR images of the tumor regions enhanced by Fe_3O_4@PEG can be used to predict the therapeutic efficacy of the micelle drugs (Scheme 1). The MION used herein were synthesized by a thermal decomposition method and decorated with DSPE-PEG2000. Our study demonstrated that this T_2-weighted contrast agent possessed superior monodispersity, optimal relaxivity, long stability, and excellent biocompatibility, which makes it suitable for *in vivo* MR imaging. We used micro-MRI in live 4T1 tumor-bearing mice to acquire the enhanced images and the enhancement intensities of the tumor tissue were quantitatively measured as TNR (Tumor/Normal tissue signal Ratio) values. The PLA-PEG/PTX micelle drug with a size smaller than that of Fe_3O_4@PEG was synthesized as a tumor inhibitor. The correlation between the delay in tumor growth and the TNR values validated that the intravenous administration of Fe_3O_4@PEG can be used to predict the therapeutic efficacy of the micelle drugs with a smaller size in a certain period of time.

Results and discussion

Characterization and purification of Fe_3O_4@PEG

Uniform oleic acid (OA) coated MION (Fe_3O_4@OA) were synthesized *via* thermal decomposition of $Fe(acac)_3$ as the iron precursor in the presence of surfactants. The hydrophobic MION could be easily transformed to an aqueous solution through rotary evaporation with DSPE-PEG. As shown in Fig. 1A, excess empty lipid micelles exist along with Fe_3O_4@PEG. Since the lipid micelles with broad size distri-

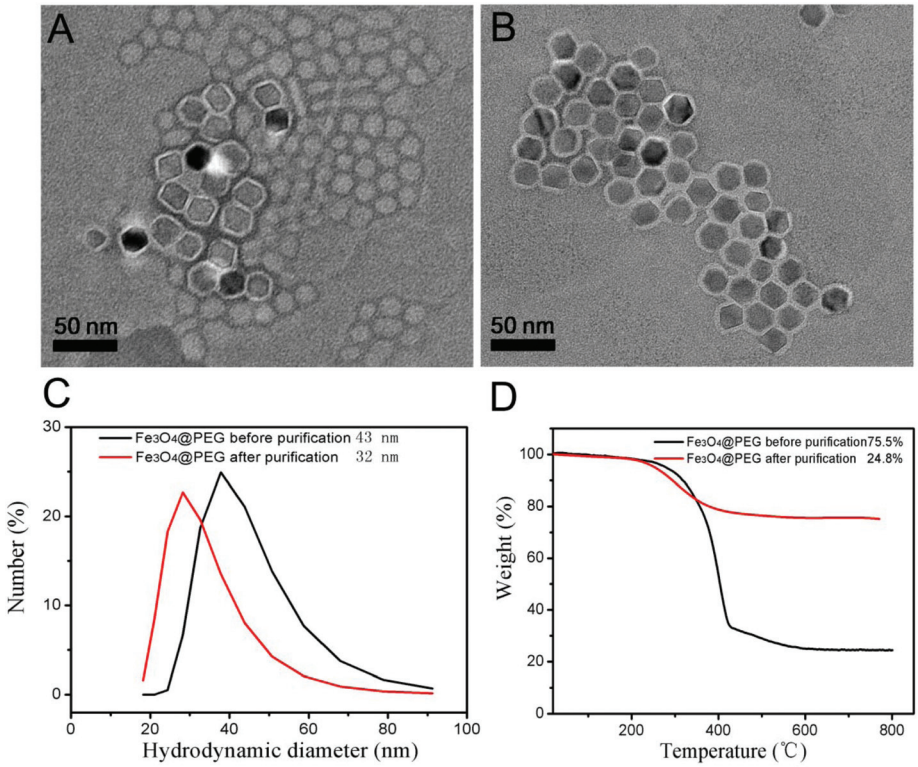

Fig. 1 TEM images of Fe_3O_4@PEG (A) before and (B) after purification. (C) DLS data and (D) TGA of Fe_3O_4@PEG before and after purification.

bution will have an adverse impact on the penetration of Fe_3O_4@PEG into the tumor mass, further purification was performed by repeated magnetic separation. The purified Fe_3O_4@PEG had a magnetic core of 22 nm and an organic shell of 3.2 nm (Fig. 1B). A comparison of the hydrodynamic diameters of Fe_3O_4@PEG before and after purification is shown in Fig. 1C, in which Fe_3O_4@PEG revealed a clearly smaller size (32 nm) post purification than that prior to purification (43 nm). TGA was performed to further confirm the purity of Fe_3O_4@PEG. As shown in Fig. 1D, the relative weight-loss of Fe_3O_4@PEG is 24.8% in contrast to that of the pre-purified Fe_3O_4@PEG (75.5%), which demonstrated that plenty of lipid micelles were removed.

It is known that the magnetism and colloidal stability of MION are significant for the *in vivo* application. As is shown in Fig. 2A, the hysteresis loop of the Fe_3O_4@PEG aqueous solution at room temperature (300 K) displayed particularly high saturation magnetization (M_s) of 94 emu g^{-1} Fe. Furthermore, the hysteresis loop exhibited favourable superparamagnetism. In the MRI measurement, the corresponding relaxivity coefficient (r_2) value was calculated to be 571 mM^{-1} s^{-1} (Fig. 2B), which was extremely high for a T_2 contrast agent. In addition, Fe_3O_4@PEG exhibited an excellent stability and morphology in an aqueous solution during a long period of time (9 months) without visible aggregation (Fig. 2C and D). Moreover, Fe_3O_4@PEG could remain stable for about 4 h in RPMI 1640 with 10% FBS, which made it feasible for *in vivo* MR imaging (Fig. S1†).

Cellular cytotoxicity and non-specific phagocytosis of Fe_3O_4@PEG

In general, a key consideration for *in vivo* use of nanomaterials is to assess their biocompatibility. In this regard, CCK8 assays using 4T1 cells and HUVECs were carried out to evaluate the cytotoxicity of Fe_3O_4@PEG at various concentrations (0–100 μg Fe per mL) for 24 h and 48 h. Fig. 3A and B present that the cell viability exceeded 90% even at a relatively high concentration of 100 μg Fe per mL, revealing the favorable biocompatibility of Fe_3O_4@PEG as a contrast agent for *in vivo* MR imaging.

In addition, the ability to resist against non-specific uptake by RES is another significant consideration for *in vivo* application.[30,31] Herein, we conducted an *in vitro* cell phagocytosis experiment using RAW 264.7 macrophages incubated with Fe_3O_4@PEG and Fe_3O_4@DMSA for comparison. Fe_3O_4@DMSA (2,3-dimercaptosuccinic acid) was used as a positive control, which could be easily phagocytosed by macrophages. After incubation for 4 h and 8 h, the macrophages were stained with Prussian blue to determine the amount of MION inside the cells. The representative images shown in Fig. 3C indicated that both Fe_3O_4@PEG and Fe_3O_4@DMSA were phagocytosed in a time-dependent way. It could be observed that nearly all the macrophages incubated with Fe_3O_4@DMSA were blue-stained after 4 h and 8 h incubation. Moreover, 4 h cocultivation with Fe_3O_4@PEG induced non-detectable cellular uptake, while 8 h cocultivation led to extremely lower cell uptake. These results confirmed that PEGylation with DSPE-PEG could dramatically minimize the non-specific phagocytosis by macrophages.

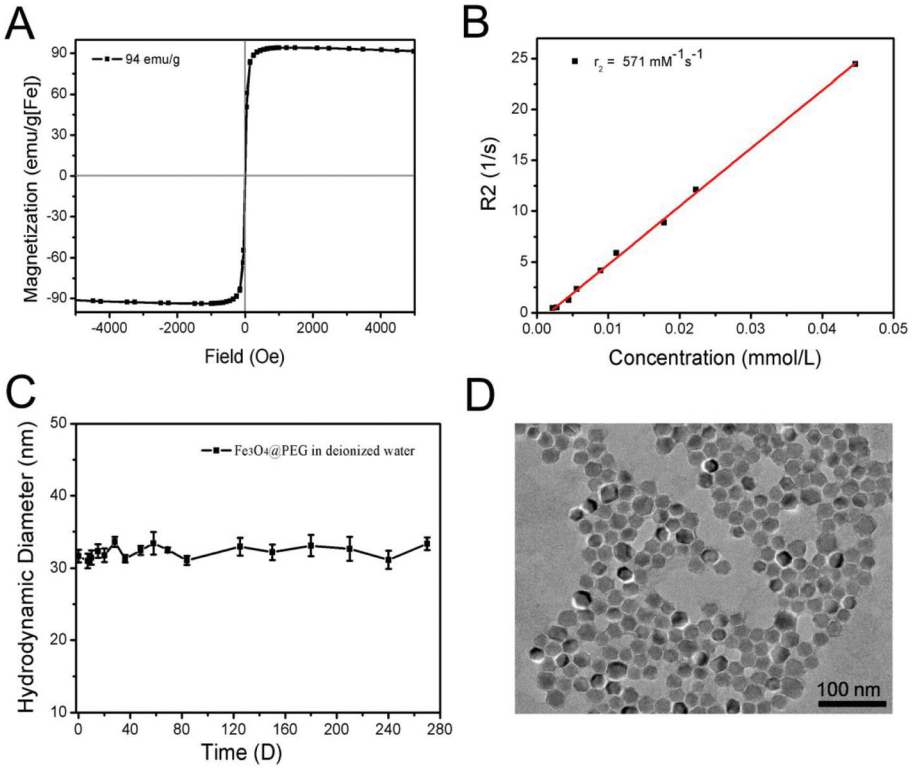

Fig. 2 (A) *M*–*H* curve of Fe_3O_4@PEG. (B) Relaxation time of Fe_3O_4@PEG *versus* iron concentration measured by a 3.0 T MR scanner. (C) Average hydrodynamic diameters of Fe_3O_4@PEG in deionized water over 9 months. The data of (C) are shown as mean ± SE (n = 3). (D) TEM image of Fe_3O_4@PEG after storage in deionized water for 9 months at 4 °C.

Distribution of Fe_3O_4@PEG in tumors detected by T_2^*-weighted MRI

The EPR effect results from larger pores on tumor blood vessels, which induce higher permeability and hydraulic conductivity in the tumor than in the normal tissues.[32] While using the EPR effect as a rationale for nano-drugs, it should be noted that not all tumor vessels are leaky, which causes heterogeneous extravasation and distribution.[11,33] As the EPR effect is the basis of nano-drug delivery, it is significant to evaluate the status of the tumor-EPR before treatment with nanomedicines. To demonstrate the EPR effect of the tumors on different mice, Fe_3O_4@PEG as a contrast agent was injected intravenously into the female BABL/c mice bearing 4T1 tumors and T_2^*-weighted MR images were acquired before and 3 h post-injection by a 7.0 T micro-MRI. Clearly, the distribution of Fe_3O_4@PEG was diverse in the tumor tissues of different mice (Fig. 4A–C). To further observe the distribution, MRI was performed on two mice with relatively large tumors of 450 and 750 mm^3. Fe_3O_4@PEG accumulated in the center (Fig. S2A†) and margin (Fig. S2B†) of the tumor. It is known that larger contrast enhancement represented better EPR effect. To assess the imaging effect, the enhancement intensity of the tumor tissue was analyzed quantitatively based on the TNR (Tumor/Normal tissue signal Ratio) values between the tumor and the adjacent normal muscle.[25,26] Then, the mice were divided into A, B, and C groups according to the calculated TNR values as TNR < 0.5, 0.5 < TNR < 0.7, and TNR > 0.7, respectively (Fig. 4D), where group A showed the best imaging enhancement. This indicates that the smaller the TNR values, the better the EPR effect.

To confirm the *in vivo* distribution of Fe_3O_4@PEG, the main organs and tumors were stained with Prussian blue and Nuclear fast red 24 h post-injection of normal saline and Fe_3O_4@PEG, respectively. The result showed that Fe_3O_4@PEG primarily accumulated in the tumor tissue as well as in the liver and the spleen based on the existence of the blue spots (Fig. S3†). In addition, hematoxylin and eosin (H&E) staining of the major organs exhibited no evidence of any adverse effects due to the presence of Fe_3O_4@PEG (Fig. S4†).

Characterization and cytotoxicity of PLA-PEG and PLA-PEG/PTX micelles

The morphology of the PLA-PEG and PLA-PEG/PTX micelles was examined by TEM (Fig. 5A and B), which showed no visible difference. Nevertheless, the PLA-PEG/PTX micelles revealed a considerably larger hydrodynamic diameter (20 nm, similar to Genexol-PM of 24 nm (ref. 9)) than that of the PLA-PEG micelles (16.5 nm, Fig. 5C), which resulted from the encapsulation of PTX. The encapsulation efficiency and drug-loading efficiency of PTX were 93.6% and 15.6%, respectively. The PLA-PEG/PTX micelles exhibited a sustained *in vitro* PTX release without any burst releases (Fig. 5D).

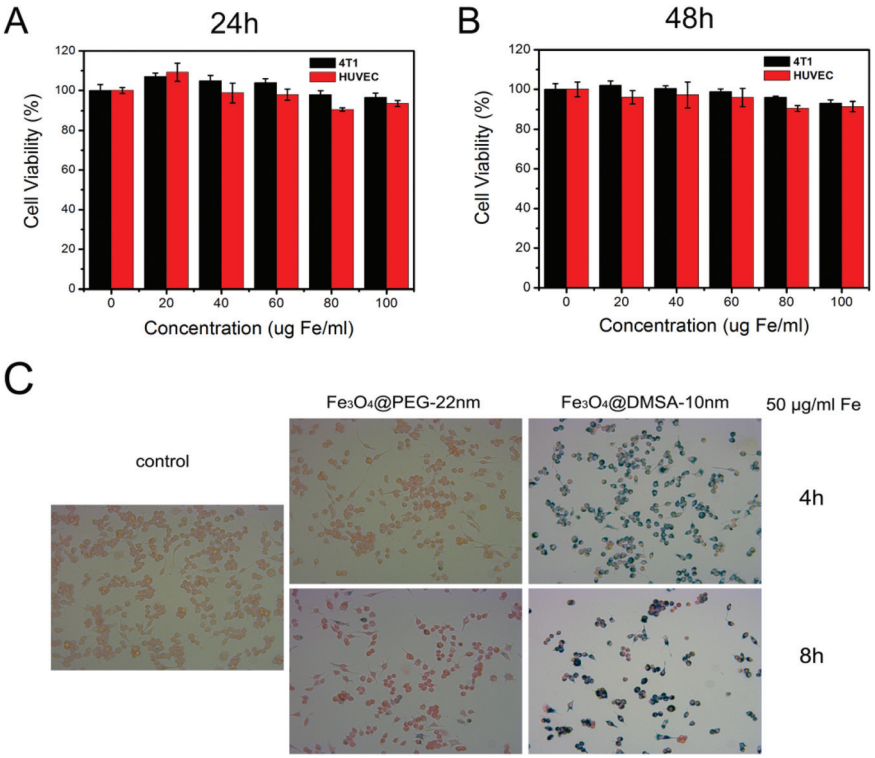

Fig. 3 (A, B) *In vitro* cytotoxicity test of Fe_3O_4@PEG against the 4T1 cells and HUVECs. The viability of the cells was determined by CCK8 assay after incubation with various concentrations of Fe for 24 h and 48 h (n = 4). (C) Cellular uptake testing with Nuclear fast red and Prussian blue double staining images (200×) of macrophages RAW 264.7 after 4 h and 8 h treatment with Fe_3O_4@PEG and Fe_3O_4@DMSA at the concentration of 50 μg Fe per ml.

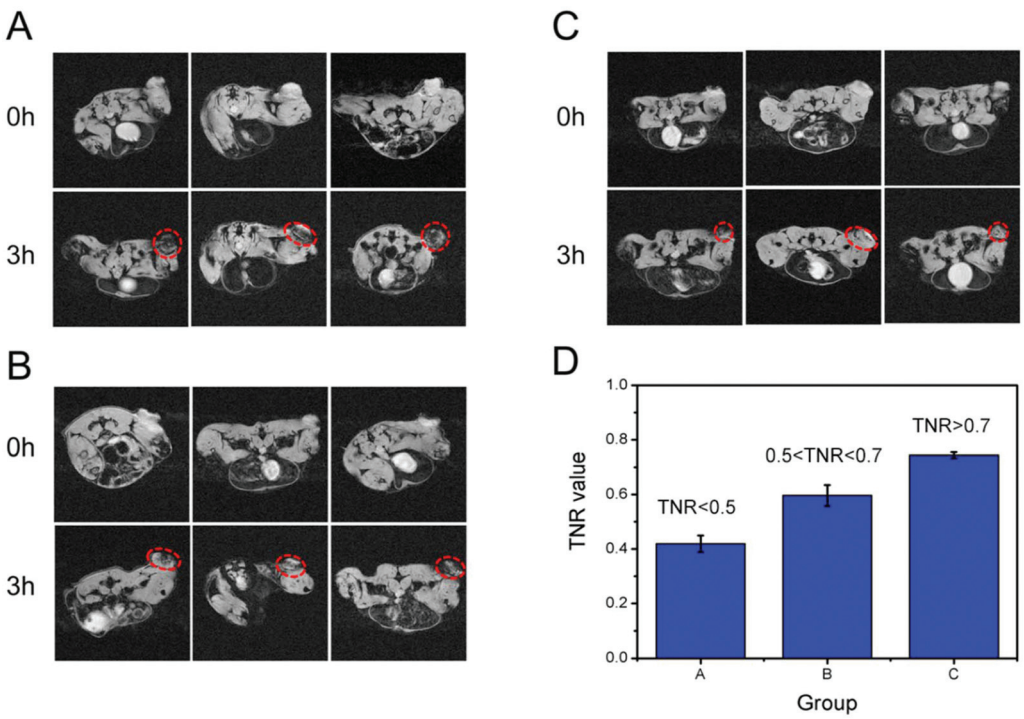

Fig. 4 (A–C) T_2^*-Weighted MR images of the mice tumor acquired before and 3 h after single tail vein injection of Fe_3O_4@PEG (30 mg Fe per kg body weight) using a 7 T MR scanner. The red dotted line displayed the tumor site. (D) TNR (Tumor/Normal tissue signal Ratio) value of MRI-based average signal in the A–C groups. The data of (D) are shown as mean ± SE (n = 3).

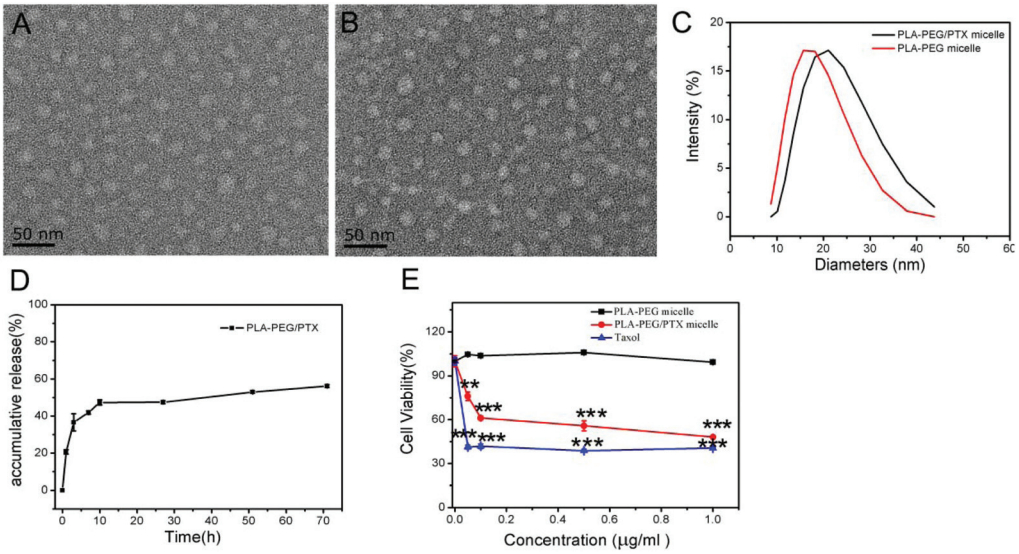

Fig. 5 TEM images of (A) PLA-PEG micelle and (B) PLA-PEG/PTX micelle. (C) DLS data of PLA-PEG micelle and PLA-PEG/PTX micelle. (D) Drug release curve of PLA-PEG/PTX micelle. PLA-PEG/PTX micelle was incubated in phosphate buffered saline (pH = 7.4) at 37 °C. (E) A cytotoxicity test of PLA-PEG micelle, PLA-PEG/PTX micelle, and Taxol against the 4T1 cells. The viability of the cells was determined by CCK8 assay after incubation with various concentrations of PTX for 24 h (n = 4). The asterisk indicated statistical significance (**p < 0.01, ***p < 0.001) of the difference in cytotoxicity between PLA-PEG/PTX micelle and the control and between Taxol and the control. The data of (D) and (E) are shown as mean ± SE.

After 24 h incubation with the 4T1 mice breast cancer cells, the PLA-PEG/PTX micelles displayed distinct cytotoxicity even at a low concentration of PTX, which was comparable with Taxol (paclitaxel chemotherapeutic drug used in the clinic) (Fig. 5E). However, the blank PLA-PEG micelles exhibited no appreciable toxicity (Fig. 5E), indicating the biocompatibility of the nanocarrier.

Inhibitory effect of PLA-PEG/PTX micelles on the tumors in different groups

As the TNR values of the MR images acquired post-injection served as the evaluation criterion of the tumor EPR effect, further experimental data was required to verify the accuracy of this assessment method. Therefore, the PLA-PEG/PTX micelles were synthesized as a chemotherapeutic drug and twelve mice bearing the 4T1 tumors were used to assess the therapeutic efficacy. First, MRI was performed to acquire the images of the tumor site after injection of the Fe_3O_4@PEG contrast agent. Then, the TNR value of each mouse was calculated and the mice were divided into three groups, A, B, and C, according to the calculated TNR values as TNR < 0.5, 0.5 < TNR < 0.7 and TNR > 0.7, respectively (Fig. 6(A–C)). The initial tumor volume in three groups is listed in Table S1† and there was no significant difference (P > 0.05) in the tumor size distribution among three groups on day 0. After intravenous treatment with the PLA-PEG/PTX micelles, the curves showing the delay of the

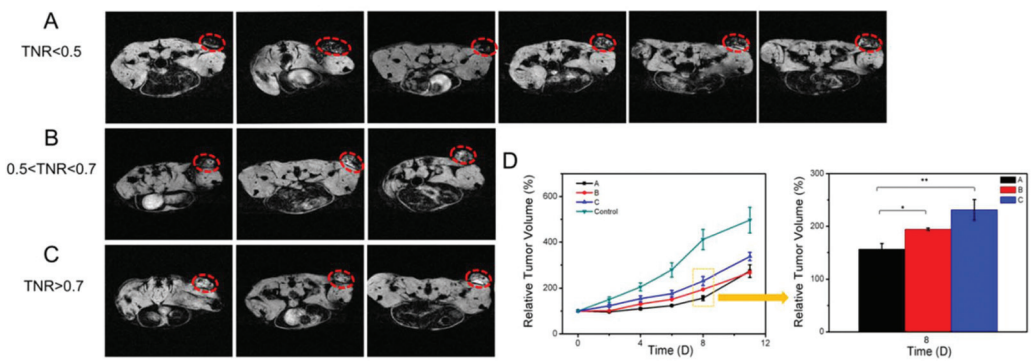

Fig. 6 (A–C) T_2^*-Weighted MR images of 12 mice tumors acquired 3 h after single tail vein injection of Fe_3O_4@PEG (30 mg Fe per kg body weight) using a 7 T MR scanner. The red dotted line displayed the tumor site. The mice were divided according to TNR. (D) Tumor growth behavior of mice in the A, B, and C groups with the repeated intravenous treatment with PLA-PEG/PTX micelle in 11 days (single dose: 60 mg PTX per kg body weight, 3 times). The data of (D) are shown as mean ± SE. The asterisk indicated statistical significance (*p < 0.05, **p < 0.01).

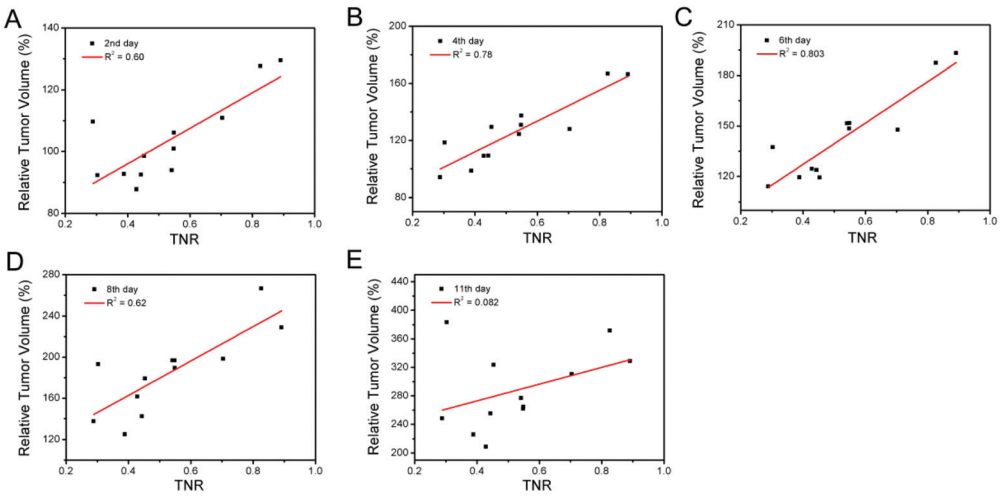

Fig. 7 The correlation between relative tumor volume of 12 mice and their TNR (Tumor/Normal tissue signal Ratio according to MR images in Fig. 6) on (A) 2nd day, (B) 4th day, (C) 6th day, (D) 8th day, and (E) 11th day after intravenous treatment with PLA-PEG/PTX micelle.

tumor growth demonstrated that group A (TNR < 0.5) exhibited the optimal inhibitory effect (Fig. 6D). In addition, the tumor inhibition in group A was notably different as compared to that in group B ($P < 0.05$, Fig. 6D) and C ($P < 0.01$, Fig. 6D). These results indicated the high potential of the excellent EPR effect (TNR < 0.5) in improving micelle-drug therapy for the tumors. However, the suppression effect in group A on day 11 did not show any significant difference as compared to that in the other two groups.

To further reveal the correlation, we performed a linear fitting between the TNR value and the relative tumor volume on day 2, 4, 6, 8, and 11 during the treatment with PLA-PEG/PTX micelles and the R^2 value was used to assess the goodness of fit. Fig. 7(A–D) revealed a superior relationship between the TNR value and the therapeutic efficacy, particularly on the 6th day of the treatment, where $R^2 = 0.803$, while the lowest correlation coefficient ($R^2 = 0.082$) was obtained on day 11 (Fig. 7E). These analysis results indicated that the TNR values calculated from the T_2^*-MR images of mice tumors enhanced by Fe_3O_4@PEG (d = 32 nm) could be used to predict the therapeutic efficacy of a nanomedicine ($d \leq$ 32 nm) in a certain period of time. Since the permeability in the tumor models varies with time and in response to the treatment,[11,34] MRI should be performed once more to afford the latest permeability situation of the tumor vessel after a period of therapy for more precise treatment with the micelle drug.

Furthermore, as the micelle drugs have a higher maximum tolerated dose than that of the traditional antineoplastic,[27] there were no adverse effects on the major organs of mice observed through H&E staining (Fig. S4†) and no significant decline of mice body weight (Fig. S5B†) even at a really high therapeutic dose of 60 mg kg^{-1}. In general, the PLA-PEG/PTX micelles displayed good tumor inhibition (Fig. S5A†). Thus, the micelle drugs may be more effective for cancer therapy.

Experimental

Synthesis of PEGylated magnetic iron oxide nanoparticles (MION)

The oleic acid (OA) coated MION were synthesized by a thermal decomposition method reported in our previous study.[23] The products were further decorated with DSPE-PEG2000 for realizing water-solublity.[24–26] In detail, DSPE-PEG2000 (powder, 45 mg, purchased from A.V.T. (Shanghai) Pharmaceutical Co. Ltd) and OA-coated MION (15 mg, iron content) were mixed and dissolved in 6 mL chloroform in a 25 mL round-bottom flask. Then, 7 mL deionized water was added to the mixture. Then, the mixture was rotary-evaporated (70 °C, 10 min) until chloroform was completely removed. The obtained PEGylated MION (Fe_3O_4@PEG) were monodispersed in water. During the surface modification, excess lipid micelles were formed simultaneously. The Fe_3O_4@PEG colloidal solution was then purified 5 times by magnetic separation to completely remove the empty lipid micelles.

Synthesis of PLA-PEG and PLA-PEG/PTX micelles

The paclitaxel-loaded biodegradable polymeric micelles were prepared by a thin-film hydration technique.[27,28] Briefly, paclitaxel (PTX, 30 mg) and PEG2000-PDLLA1750 (150 mg, purchased from Shanghai Ponsure Biotech, Inc.) were dissolved in 2 mL acetonitrile. After being stirred for 5 min, the organic solvent was evaporated (60 °C, 20 min) by rotary-evaporation to obtain a yellowish transparent thin film, which was then kept in vacuum overnight at 40 °C to completely remove the residual solvent. The resultant film was dissolved by adding 5 mL deionized water at 60 °C and stirring for 10 min to obtain a transparent micelle solution. Then, the solution was filtered through a 0.22 μm filter to remove the unincorporated PTX and stored at 4 °C. The synthesis of the PLA-PEG micelles was the same as above, but without the addition of PTX.

Characterization of Fe_3O_4@PEG, PLA-PEG, and PLA-PEG/PTX micelles

The morphology of Fe_3O_4@PEG before and after purification and the morphology of PLA-PEG and PLA-PEG/PTX micelles were examined using a transmission electron microscope (TEM, Tokyo JEOL, Japan). Fe_3O_4@PEG and the micelles were negatively stained with 2% phosphotungstic acid to indicate the coating polymer. The hydrodynamic diameters of Fe_3O_4@PEG in an aqueous solution before and after purification and the size of PLA-PEG and PLA-PEG/PTX micelles were measured with a particle size analyzer (Malvern ZS90, UK). The thermal behavior of the powders of Fe_3O_4@PEG before and after purification was studied by thermogravimetric analysis (TGA) using a Thermo Gravimetric Analyzer (Pyris 1 DSC, USA). The iron concentration of Fe_3O_4@PEG was measured by the 1,10-phenanthroline spectrophotometric method on a UV-visible spectrophotometer (UV-3600, Shimadzu, Japan).[29] The magnetism of Fe_3O_4@PEG was obtained by a vibrating sample magnetometer (VSM, Lakeshore 7407, USA) at room temperature. The T_2 relaxation property of Fe_3O_4@PEG was investigated on a clinical 3.0 T MR scanner (Avanto, Siemens, Germany). The concentration of PTX in the PLA-PEG/PTX micelle solution was determined with HPLC (LC20AD, Shimadzu, Japan) at 228 nm. The release behavior of the PLA-PEG/PTX micelles was detected against phosphate buffered saline (PBS, 0.01 M, pH7.4) with 0.5% Tween 80 at 37 °C *in vitro* and the released drug was measured by HPLC at different time-points.

Cellular cytotoxicity and uptake

The CCK8 assay was used to evaluate the cytotoxicity of Fe_3O_4@PEG and the PLA-PEG/PTX micelle. In the cytotoxicity test of Fe_3O_4@PEG, the 4T1 cells and HUVECs were incubated in the 96-well plates at a density of 1×10^4 cells per well, grown overnight (n = 4), and incubated with a series of concentrations (0–100 μg Fe per ml) of Fe_3O_4@PEG at 37 °C for 24 h and 48 h. For the PLA-PEG/PTX micelles, the 4T1 cells were used to evaluate the cytotoxicity. The 4T1 cells were seeded onto the 96-well plates with 1×10^4 cells per well, grown overnight, and subsequently incubated with the PLA-PEG micelles, PLA-PEG/PTX micelles, and Taxol (paclitaxel) at a series of concentrations (0–1 μg PTX per ml) for 24 h.

The RAW 264.7 macrophages were used to detect the cell-uptake of Fe_3O_4@PEG. Comparatively, the macrophages were treated with Fe_3O_4@PEG and Fe_3O_4@DMSA at a concentration of 50 μg Fe per mL in the 12-well plates for 4 h and 8 h. After 4 h and 8 h incubation at 37 °C, the cells were washed with PBS for 3 times and fixed with 4% paraformaldehyde for 30 min. Prussian blue staining was used to determine the intracellular iron, followed by counter-staining with Nuclear fast red. The cells were placed on an inverted microscope for cellular non-specific phagocytosis observation.

Animal protocol

Female BALB/c mice aged 4–6 weeks (18–22 g in weight) were purchased from the Model Animal Research Center of Southeast University. All animal care and experimental procedures were performed in compliance with the Animal Experimentation Guidelines and with the approval of the Animal Care Committee at Southeast University, Najing, China. To establish the experimental model of a breast tumor, the 4T1 cells (2×10^6 cells in 200 μl PBS) were subcutaneously injected into the right flanks of the mice. Seven days after injection, when the tumor grew to probably 100 mm^3, the mice were used for MR diagnostics.

In vivo MRI experiments

In vivo MR imaging of Fe_3O_4@PEG on the tumor site was performed using a 7.0 T micro-MRI (PharmaScan, Bruker, Germany) with a 38 mm circular coil and a mouse cradle. The mice were initially anesthetized with a 4% isoflurane/air gas mixture. MR imaging was conducted prior to tail vein injection and 3 h post-injection of Fe_3O_4@PEG (30 mg Fe per kg body weight). The T_2^*-weighted MR images of the mice tumor were acquired. The scan parameters were as follows: TR/TE = 400 ms/8.0 ms for T_2^*-weighted flash sequence, field of view = 6 cm, flip angle = 30°, FOV = 3.2 cm × 3.2 cm, slice thickness = 1 mm, and matrix size = 256 × 256.

In vivo antitumor assay with the PLA-PEG/PTX micelles

The treatments were carried out when the tumor on the mice reached a volume of 100–200 mm^3 and this day was designated as day 0. The mice were treated intravenously with the PLA-PEG/PTX micelles with a single dose of 60 mg per kg per day on 0, 4th, and 8th day. The tumor volumes were calculated using the formula of $V = AB^2\pi/6$, where A and B are the longer and shorter diameters, respectively. The mice body weight and the tumor volume were measured every 2 days. The relative tumor volume was calculated as $100 \times V_i/V_0$, where V_i is the calculated volume and V_0 is the initial volume on day 0. The relative body weight was calculated as $100 \times m_i/m_0$, where m_i is the calculated weight and m_0 is the initial weight on day 0.

Histochemical examination

For histochemical examination of MR imaging test, the tumor tissues and the main organs of the mice were harvested 24 h after injection of Fe_3O_4@PEG. After being fixed in 10% formalin, the tissues were embedded into paraffin and sliced into 5 μm thickness. The tissue slices were stained with Prussian blue and Nuclear fast red along with Hematoxylin and Eosin (H&E).

For the antitumor assay, the main mice organs were harvested on day 11 after the measurement and processed as above and stained with H&E.

Statistical analysis

All data were reported as mean ± SE. Significant differences were determined using unpaired t-test, where the differences were considered significant when $P < 0.05$. The data were indicated with (*) for $P < 0.05$, (**) for $P < 0.01$, and (***) for $P < 0.001$.

Linear fitting was performed to evaluate the relationship between the delay in the tumor growth and the TNR values. The R^2 value was used to assess the correlation.

Conclusions

In summary, we successfully developed a novel strategy for predicting the therapeutic micelle-drug efficacy using Fe_3O_4@PEG to describe the EPR effect of the tumor tissue. Herein, the synthesized Fe_3O_4@PEG possessed relatively high r_2 of 571 mM^{-1} s^{-1} and high saturation magnetization of 94 emu g^{-1} Fe. In addition, the external PEGylation shell effectively reduced non-specific phagocytosis and improved biocompatibility. The stability studies exhibited that Fe_3O_4@PEG could maintain favorable morphology and monodispersity in deionized water for 9 months with small changes in the hydrodynamic diameter. The TNR values, which were measured based on the MR images of the mice tumors acquired after intravenous administration of Fe_3O_4@PEG with a diameter of 32 nm, were proven to be able to predict the therapeutic efficacy of the micelle drugs with a diameter smaller than 32 nm in a certain period of time. Therefore, we believe that Fe_3O_4@PEG can be used as an ideal contrast agent for T_2^*-weighted MR imaging to describe the EPR effect of the tumors in the patients for accurate medication guidance in the future.

Conflicts of interest

The authors declare no competing financial interest.

Acknowledgements

This research was supported by the National Key Research and Development Program of China (no. 2017YFA0205502), the National Basic Research Program of China (973 program no. 2013CB733800), National Natural Science Foundation of China (no. 81571806, 81671820, and 81301870), the Jiangsu Provincial Special Program of Medical Science (BL2013029), and the Fundamental Research Funds for the Central Universities.

Notes and references

1 V. Wagner, A. Dullaart, A.-K. Bock and A. Zweck, *Nat. Biotechnol.*, 2006, **24**, 1211–1217.
2 J. C. Kraft, J. P. Freeling, Z. Wang and R. J. Ho, *J. Pharm. Sci.*, 2014, **103**, 29–52.
3 N. Kamaly, Z. Xiao, P. M. Valencia, A. F. Radovic-Moreno and O. C. Farokhzad, *Chem. Soc. Rev.*, 2012, **41**, 2971–3010.
4 F. Yuan, M. Leunig, S. K. Huang, D. A. Berk, D. Papahadjopoulos and R. K. Jain, *Cancer Res.*, 1994, **54**, 3352–3356.
5 J. Luo, K. Xiao, Y. Li, J. S. Lee, L. Shi, Y.-H. Tan, L. Xing, R. Holland Cheng, G.-Y. Liu and K. S. Lam, *Bioconjugate Chem.*, 2010, **21**, 1216–1224.
6 J. K. Valenzuela-Oses, M. C. García, V. A. Feitosa, J. A. Pachioni-Vasconcelos, S. M. Gomes-Filho, F. R. Lourenço, N. N. Cerize, D. S. Bassères and C. O. Rangel-Yagui, *Mater. Sci. Eng., C*, 2017, **81**, 327–333.
7 J. Zhang, H. Kinoh, L. Hespel, X. Liu, S. Quader, J. Martin, T. Chida, H. Cabral and K. Kataoka, *J. Controlled Release*, 2017, **264**, 127–135.
8 K. S. Lee, H. C. Chung, S. A. Im, Y. H. Park, C. S. Kim, S.-B. Kim, S. Y. Rha, M. Y. Lee and J. Ro, *Breast Cancer Res. Treat.*, 2008, **108**, 241–250.
9 M. E. Werner, N. D. Cummings, M. Sethi, E. C. Wang, R. Sukumar, D. T. Moore and A. Z. Wang, *Int. J. Radiat. Oncol., Biol., Phys.*, 2013, **86**, 463–468.
10 R. K. Jain and T. Stylianopoulos, *Nat. Rev. Clin. Oncol.*, 2010, **7**, 653–664.
11 F. Yuan, Y. Chen, M. Dellian, N. Safabakhsh, N. Ferrara and R. K. Jain, *Proc. Natl. Acad. Sci. U. S. A.*, 1996, **93**, 14765–14770.
12 N. Bertrand, J. Wu, X. Xu, N. Kamaly and O. C. Farokhzad, *Adv. Drug Delivery Rev.*, 2014, **66**, 2–25.
13 M. Koukourakis, S. Koukouraki, A. Giatromanolaki, S. Archimandritis, J. Skarlatos, K. Beroukas, J. Bizakis, G. Retalis, N. Karkavitsas and E. Helidonis, *J. Clin. Oncol.*, 1999, **17**, 3512–3521.
14 L. Song, F. Zang, M. Song, G. Chen and Y. Zhang, *J. Nanosci. Nanotechnol.*, 2015, **15**, 4111–4118.
15 D. Kokuryo, Y. Anraku, A. Kishimura, S. Tanaka, M. R. Kano, J. Kershaw, N. Nishiyama, T. Saga, I. Aoki and K. Kataoka, *J. Controlled Release*, 2013, **169**, 220–227.
16 N. Lee, Y. Choi, Y. Lee, M. Park, W. K. Moon, S. H. Choi and T. Hyeon, *Nano Lett.*, 2012, **12**, 3127–3131.
17 H. Wu, L. Song, L. Chen, Y. Huang, Y. Wu, F. Zang, Y. An, H. Lyu, M. Ma and J. Chen, *Nanoscale*, 2017, **9**, 16175–16182.
18 R. Qiao, C. Yang and M. Gao, *J. Mater. Chem.*, 2009, **19**, 6274–6293.
19 J. Park, E. Lee, N. M. Hwang, M. Kang, S. C. Kim, Y. Hwang, J. G. Park, H. J. Noh, J. Y. Kim and J. H. Park, *Angew. Chem.*, 2005, **117**, 2932–2937.
20 N. Lee, H. Kim, S. H. Choi, M. Park, D. Kim, H.-C. Kim, Y. Choi, S. Lin, B. H. Kim and H. S. Jung, *Proc. Natl. Acad. Sci. U. S. A.*, 2011, **108**, 2662–2667.
21 H. Yang, T. Ogawa, D. Hasegawa and M. Takahashi, *J. Appl. Phys.*, 2008, **103**, 07D526.
22 M. A. Miller, S. Gadde, C. Pfirschke, C. Engblom, M. M. Sprachman, R. H. Kohler, K. S. Yang, A. M. Laughney, G. Wojtkiewicz and N. Kamaly, *Sci. Transl. Med.*, 2015, **7**, 314ra183.
23 J. Xie, C. Yan, Y. Zhang and N. Gu, *Chem. Mater.*, 2013, **25**, 3702–3709.
24 J. Xie, Y. Zhang, C. Yan, L. Song, S. Wen, F. Zang, G. Chen, Q. Ding, C. Yan and N. Gu, *Biomaterials*, 2014, **35**, 9126–9136.

25 J. Xie, C. Yan, Y. Yan, L. Chen, L. Song, F. Zang, Y. An, G. Teng, N. Gu and Y. Zhang, *Nanoscale*, 2016, **8**, 16902–16915.
26 L. Chen, J. Xie, H. Wu, F. Zang, M. Ma, Z. Hua, N. Gu and Y. Zhang, *Colloids Surf., B*, 2018, **161**, 339–346.
27 S. C. Kim, D. W. Kim, Y. H. Shim, J. S. Bang, H. S. Oh, S. W. Kim and M. H. Seo, *J. Controlled Release*, 2001, **72**, 191–202.
28 Z. Fan, C. Chen, X. Pang, Z. Yu, Y. Qi, X. Chen, H. Liang, X. Fang and X. Sha, *PLoS One*, 2015, **10**, e0120129.
29 M. Song, Y. Zhang, S. Hu, L. Song, J. Dong, Z. Chen and N. Gu, *Colloids Surf., A*, 2012, **408**, 114–121.
30 D. Liu, W. Wu, J. Ling, S. Wen, N. Gu and X. Zhang, *Adv. Funct. Mater.*, 2011, **21**, 1498–1504.
31 Z. Jia, L. Song, F. Zang, J. Song, W. Zhang, C. Yan, J. Xie, Z. Ma, M. Ma and G. Teng, *Theranostics*, 2016, **6**, 1780.
32 L. E. Gerlowski and R. K. Jain, *Microvasc. Res.*, 1986, **31**, 288–305.
33 F. Yuan, M. Dellian, D. Fukumura, M. Leunig, D. A. Berk, V. P. Torchilin and R. K. Jain, *Cancer Res.*, 1995, **55**, 3752–3756.
34 D. Fukumura, F. Yuan, W. L. Monsky, Y. Chen and R. K. Jain, *Am. J. Pathol.*, 1997, **151**, 679.